Electronic Supplementary Material (ESI) for Soft Matter.

Supporting Information 2

Rotational and translational diffusion of biomolecules in complex liquids and HeLa cells

Jarosław Michalski, Tomasz Kalwarczyk, Karina Kwapiszewska, Andrzej Poniewierski, Aneta Karpińska, Karolina Kucharska, Robert Hołyst and

Institute of Physical Chemistry, Polish Academy of Sciences Kasprzaka 44/52, 01-224 Warsaw, Poland

Jörg Enderlein

Third Institute of Physics - Biophysics, Georg August University, Friedrich-Hund-Platz 1, 37077 Göttingen, Germany

(Dated: June 6, 2024)

2.1 Plots of Sulfo-Cy5 stained CCMV particles in virus buffer

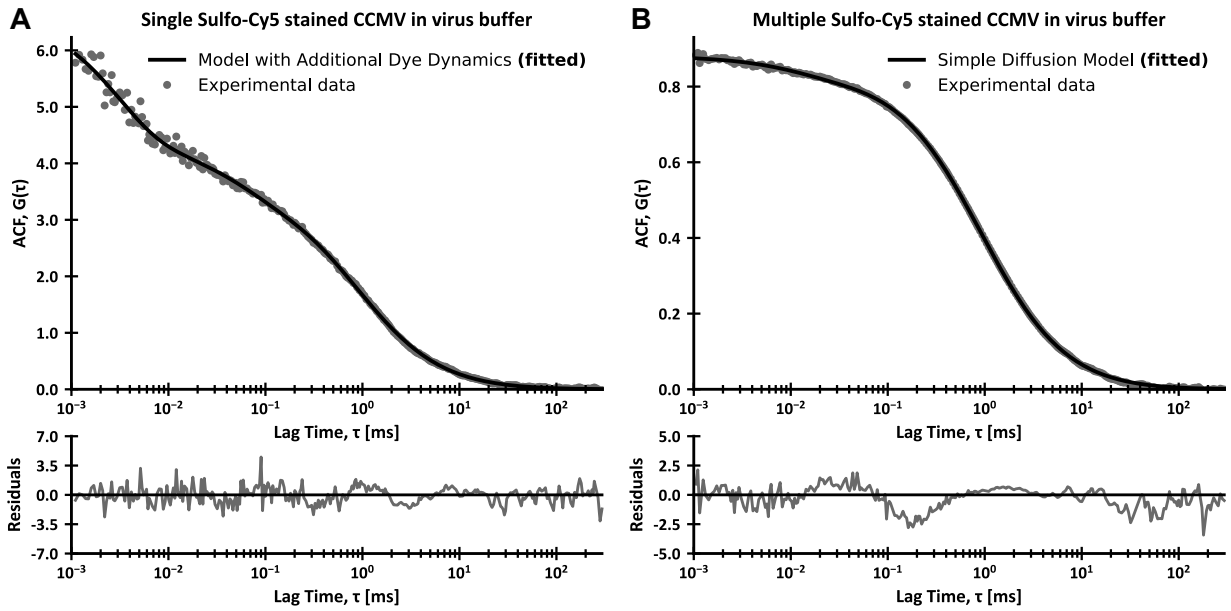

Figure S1. *(**A**) FCS data obtained for single Sulfo-Cy5 stained CCMV particles in virus buffer (viscosity equal to water) at 25 °C. The experimental data was fitted with a model including translational diffusion and coupling of rotational diffusion with first-order dynamics (Eq. 15), achieving a good fit. (**B**) FCS data obtained for multiple Sulfo-Cy5 stained CCMV particles in the virus buffer at 25 °C. The experimental data was fitted with a simple diffusion model (Eq. 13) containing translational diffusion and triplet sates dynamics. The residuals were calculated as a difference between experimental and theoretical values divided by errors of experimental values for each datapoint.*

2.2 Alternative analysis of the experimental data of CCMV diffusion in virus buffer

On Figure S2 we show alternative analyses of the experimental data for the diffusion of single Sulfo-Cy5 stained CCMV particles in virus buffer. There we assume that the third component on the auto-correlation curve, visible between the rotational and translational diffusion results only from the triplet states dynamics. We analysed the data with a model given by Eq. S1:

$$G(\tau) = G(0)G_D(\tau)G_R(\tau)G_t(\tau) \qquad \text{(S1)}$$

$$G(0) = \frac{1}{N}$$

$$G_D(\tau) = \left[1 + \frac{\tau}{\tau_T}\right]^{-1}\left[1 + \frac{\tau}{\kappa^2\tau_T}\right]^{-\frac{1}{2}} \qquad \text{(translational motion)}$$

$$G_R(\tau) = 1 + A\exp(-6D_R\tau) \qquad \text{(rotational motion)}$$

$$G_t(\tau) = 1 + \frac{T_{Triplet}}{1-T_{Triplet}}\exp\left(-\frac{\tau}{\tau_{Triplet}}\right) \qquad \text{(triplet states dynamics)}$$

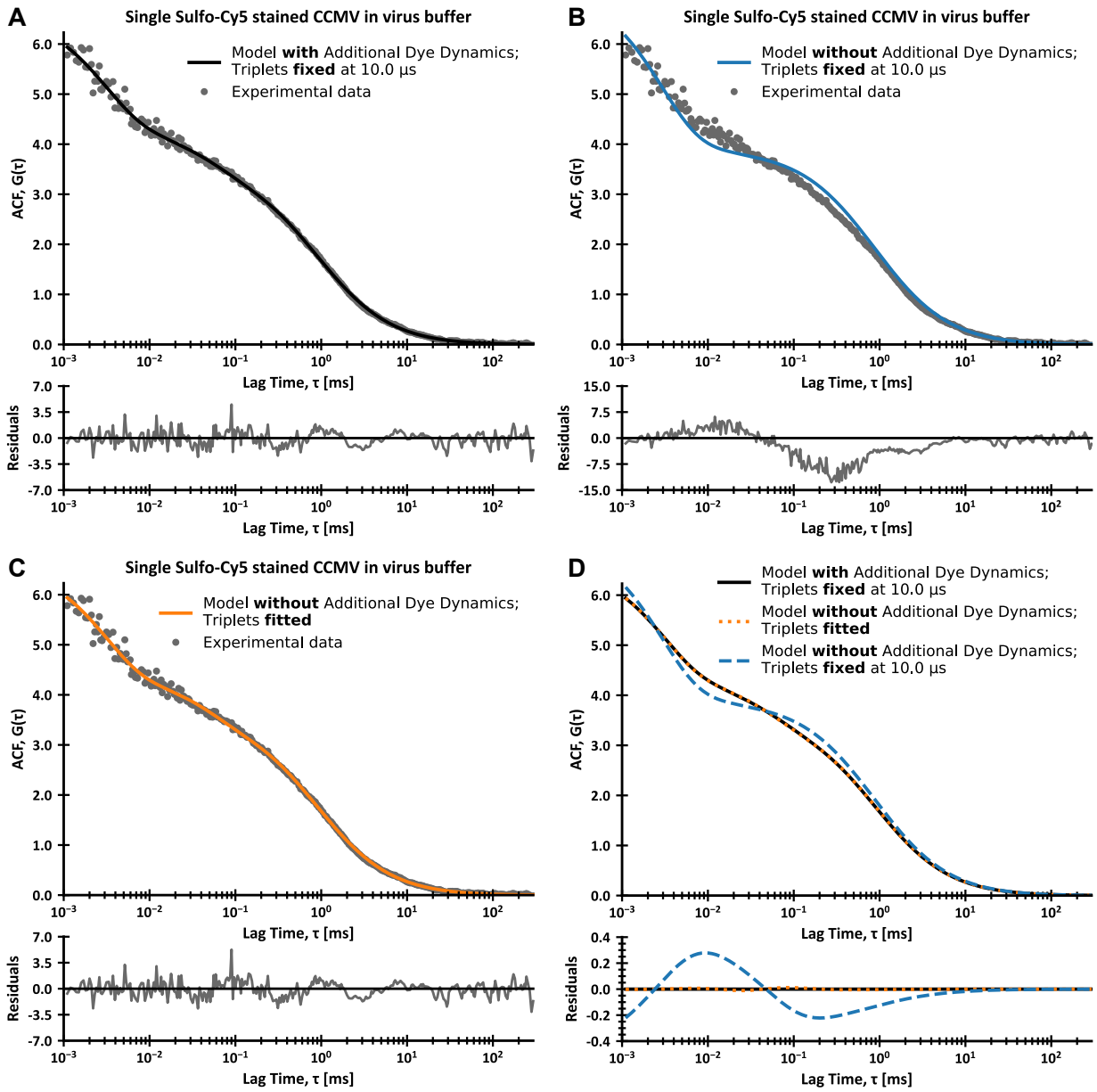

Figure S2. *(**A**-**C**) FCS data obtained for single Sulfo-Cy5 stained CCMV particles in virus buffer (viscosity equal to water) at 25 °C. (**A**) The experimental data was fitted with a model including translational diffusion and coupling of rotational diffusion with first-order dynamics (Eq. 15) with triplet states dynamics fixed at 10 µs (Table 1), achieving a good fit. (**B**) The experimental data was fitted with a model - Eq. S1 with triplet states dynamics fixed at 10 µs (Table 1), achieving a poor fit. (**C**) The experimental data was fitted with a model - Eq. S1 with triplet states dynamics as fitting parameters, achieving a good fit. The residuals on (**A**-**C**) were calculated as a difference between experimental and theoretical values divided by errors of experimental values for each datapoint. (**D**) shows a comparison of the theoretical values from (**A**-**C**). The residuals on (**D**) were calculated as a difference between values from (**A**) and (**B**) or (**C**) respectively.*

Firstly we took the values for $T_{Triplet}$ and $\tau_{Triplet}$ from the analysis of multiple stained CCMV particles in virus buffer (Table 1), with A (rotational diffusion amplitude) and r (hydrodynamic radius) as fitting

parameters (τ_T and D_R are functions of r – Eq. 11, Eq. 3). This resulted in a poor fit (Figure S2B). Then we repeated the analysis but with $T_{Triplet}$ and $\tau_{Triplet}$ as fitting parameters obtaining a good fit (Figure S2C). We also performed the same analysis for single Alexa647 stained probes with similar results.

As shown on Figure SI2D the obtained theoretical curves from Eq. 15 (coupling of rotational diffusion and dye dynamics) with fixed triplets at 10 μs and Eq. S1 with fitted triplets (without dye dynamics) are almost indistinguishable and both results in fit of high quality. As such we cannot definitely conclude which alternative is correct. However, the most important fact is that this uncertainty does not affect the parts of auto-correlation curves (experimental results) originating from the studied translational and rotational diffusion (Figure 3A). That is why it does not affect the major topic and conclusions of this work.

All the results from the analysis of single Sulfo-Cy5 and single Alexa647 stained CCMV particles are given in Table S1. In **Supporting Information 2.4** we show the analysis of the experimental data from Figure 4 and Figure 5 using the model without dye dynamics – Eq. S1 and values of parameters from Table S1 (triplets fitted).

Table S1. *The parameters of CCMV-derived probes from fitting experimental data obtained from measurements in the virus buffer at 25 °C with Eq. S1.*

	single Alexa647 stained		single Sulfo-Cy5 stained	
	Triplets fixed	Triplets fitted	Triplets fixed	Triplets fitted
r [nm]	16.4 ± 0.6	15.8 ± 0.7	15.1 ± 0.7	14.4 ± 0.9
A	0.59 ± 0.02	0.41 ± 0.02	0.76 ± 0.03	0.50 ± 0.06
$\tau_{Triplet}$ [μs]	10.0 (fixed)	36.3 ± 7.5 (fitted)	10.0 (fixed)	36.0 ± 2.1 (fitted)
$T_{Triplet}$	0.056 (fixed)	0.17 ± 0.01 (fitted)	0.056 (fixed)	0.21 ± 0.03 (fitted)

2.3 Calculation of length-scale viscosity for aqueous polyethylene glycol solutions

The values of the parameters of the LSVM for aqueous polyethylene glycol solution (Eq. 7-8), except for γ, were taken from the paper by *Wisniewska et al.*[1]: η_0 = 0.89 mPa·s; a = 1.29 (for the non-entangled regime, $R_h < \xi$) or a = 0.78 (for the entangled regime, $R_h > \xi$); R_h is given by Eq. S2; ξ is given by Eq. S3:

$$R_h = 0.0145 {M_n}^{0.571} \tag{S2}$$

$$\xi = R_g \left(\frac{c}{c^*}\right)^{-\frac{3}{4}} \tag{S3}$$

Here M_n is the number average molecular weight of the used polymer, R_g is the radius of gyration of the used polymer given by Eq. S4, c is the concentration of the used polymer, and c^* is the overlap concentration of the used polymer given by Eq. S5.

$$R_g = 0.0215 {M_n}^{0.583} \tag{S4}$$

$$c^* = \frac{M_n}{\frac{4}{3}\pi {R_g}^3 N_A} \tag{S5}$$

N_A is the Avogadro constant.

The value of the γ parameter was determined as 2.58 ± 0.20 kJ/mol based on FCS measurements of multiply Sulfo-Cy5 stained probes in a series of PEG/PEO solutions in virus buffer. We fitted the FCS data with Eq. 13. We used the value of hydrodynamic radius obtained from FCS measurements in virus buffer for multiply Sulfo-Cy5 stained probes (Table 1.) and calculated the effective viscosity for translational motion experienced by measured CCMV particles according to Eq. 2 and 11. The experimental results are presented in Table S2.

Table S2. *Experimental results from translational diffusion measurements of multiply Sulfo-Cy5 stained probes in a series of PEG/PEO solutions in virus buffer at 25 °C.*

Polymer	M_n [g/mol]	c [g/cm^3]	η_{eff}^T [mPa·s] (measured by FCS)
PEG 6 kDa	5900	0.050	1.51 ± 0.03
PEG 8 kDa	8400	0.053	1.88 ± 0.10
PEG 43 kDa	43100	0.009	1.19 ± 0.07
PEG 92 kDa	91800	0.010	1.59 ± 0.06
PEG 196 kDa	196000	0.010	1.84 ± 0.09

Next, we rewrite Eq. 7 as a dependence of $RTln\left(\frac{\eta_{eff}^T}{\eta_0}\right)$ on $\left(\frac{R_{eff}}{\xi}\right)^a$:

$$RTln\left(\frac{\eta_{eff}^T}{\eta_0}\right) = \gamma\left(\frac{R_{eff}}{\xi}\right)^a$$

It is a linear function with a slope equal to γ. Finally, we fit the experimental data to obtain the value of the gamma parameter –2.58 ± 0.20 kJ/mol (Figure S3).

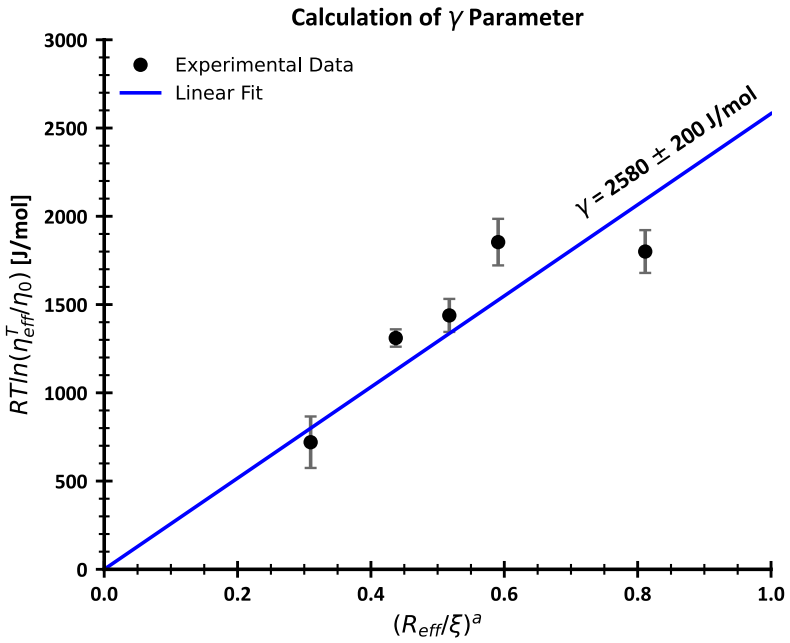

Figure S3. *FCS data for multiply Sulfo-Cy5 stained CCMV particles in solutions of PEG 6 kDa of various molecular weights in virus buffer at 25 ° C. Data presented as a* linear dependence of $RT\ln\left(\eta_{eff}^{T}/\eta_0\right)$ *on* $\left(R_{eff}/\xi\right)^{a}$ *with* γ *as slope.*

2.4 Alternative analysis of the experimental data of CCMV diffusion in polymer solutions

Similarly to the subsection **"Diffusion of CCMV plant viruses in polymer solutions"** we compared the experimental data with theoretical curves obtained from Eq. S1 and values of τ_T and D_R calculated using Eq. 2, 7-9, and 11. The parameters of the LSVM are presented in **Supporting Information 2.3.** We used the values of A, $\tau_{Triplet}$, $T_{Triplet}$ and r obtained from the analysis of FCS data from measurements in the virus buffer (Table S1, triplets fitted). We did not perform any data fitting, only normalized the ACF curves to exclude the influence of samples' concentrations.

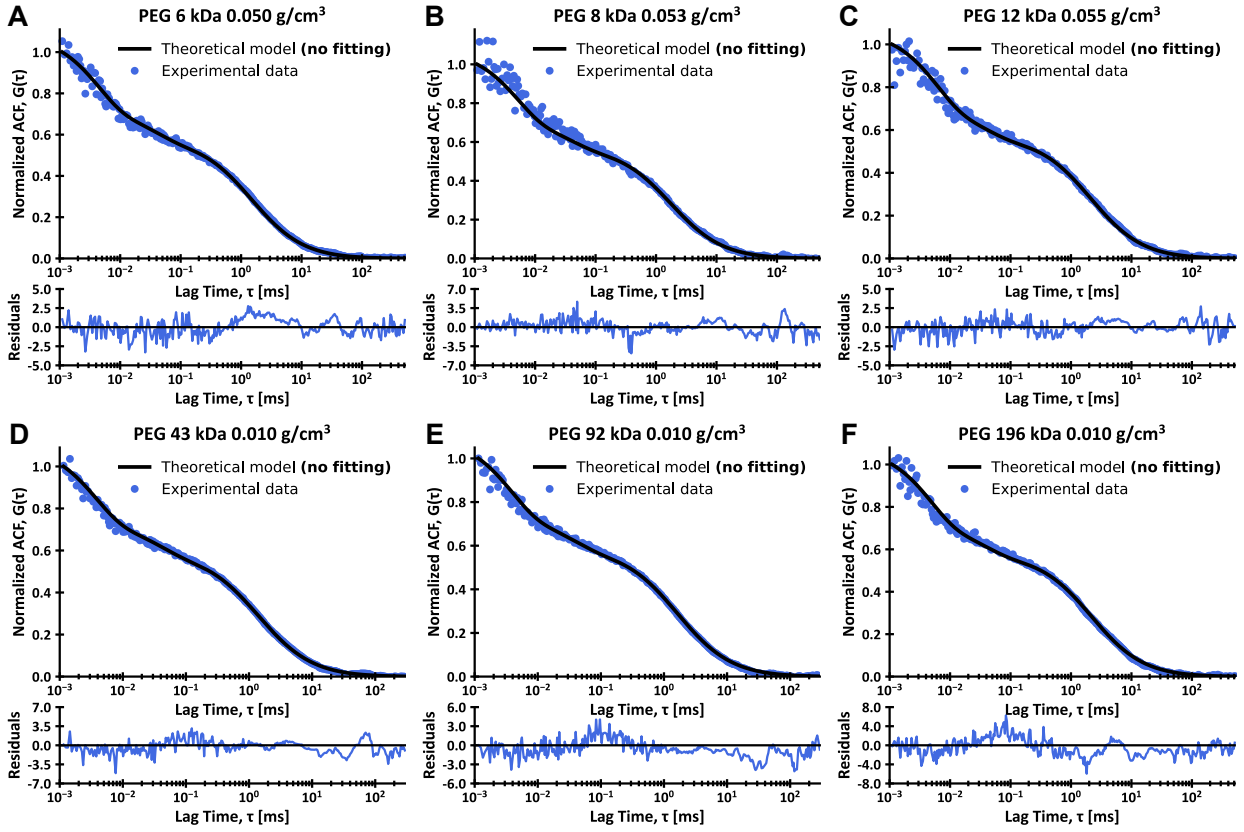

Figure S4. *FCS data for single Sulfo-Cy5 stained CCMV particles in solutions of PEG of various molecular weights in virus buffer at 25 °C and calculated theoretical curves, with plots of residues. (A) Data for 0.050 g/cm3 solution of PEG 6 kDa in virus buffer. (B) Data for 0.053 g/cm3 solution of PEG 8 kDa in virus buffer. (C) Data for 0.055 g/cm3 solution of PEG 12 kDa in virus buffer. (D) Data for 0.010 g/cm3 solution of PEG 43 kDa in virus buffer. (E) Data for 0.010 g/cm3 solution of PEG 92 kDa in virus buffer. (F) Data for 0.010 g/cm3 solution of PEG 196 kDa in virus buffer. Data presented as solid lines are not fits and were calculated according to Eq. 2, 7-9, 11, and S1. The residuals were calculated as a difference between experimental and theoretical values divided by errors of experimental values for each datapoint. The above-given values of polymer molecular weights are the number average molecular weights.*

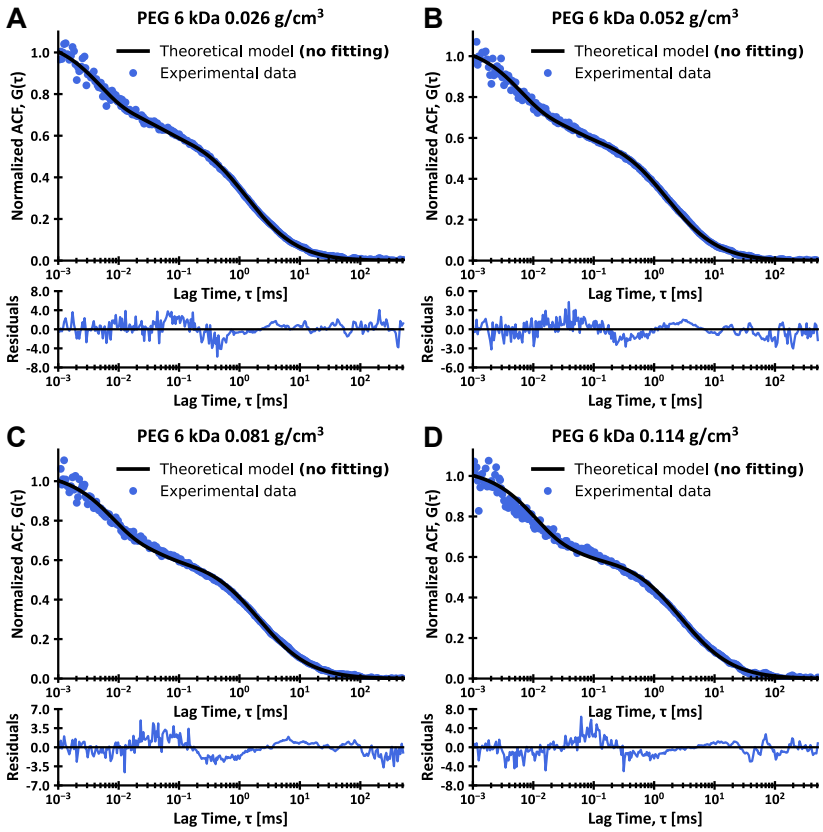

Figure S5. *FCS data for single Alexa647 stained CCMV particles in solutions of PEG 6 kDa of various concentrations in virus buffer at 25 °C and calculated theoretical curves, with plots of residues. (**A**) Data for 0.020 g/cm^3 solution of PEG 6 kDa in virus buffer. (**B**) Data for 0.049 g/cm^3 solution of PEG 6 kDa in virus buffer. (**C**) Data for 0.081 g/cm^3 solution of PEG 6 kDa in virus buffer. (**D**) Data for 0.110 g/cm^3 solution of PEG 6 kDa in virus buffer. Data presented as solid lines are **not fits** and were calculated according to Eq. 2, 7-9, 11, and S1. The residuals were calculated as a difference between experimental and theoretical values divided by errors of experimental values for each datapoint. The above-given values of polymer molecular weights are the number average molecular weights.*

2.5 Plots of Alexa 647 stained CCMV particles in PEG solutions displaying aggregation of probes

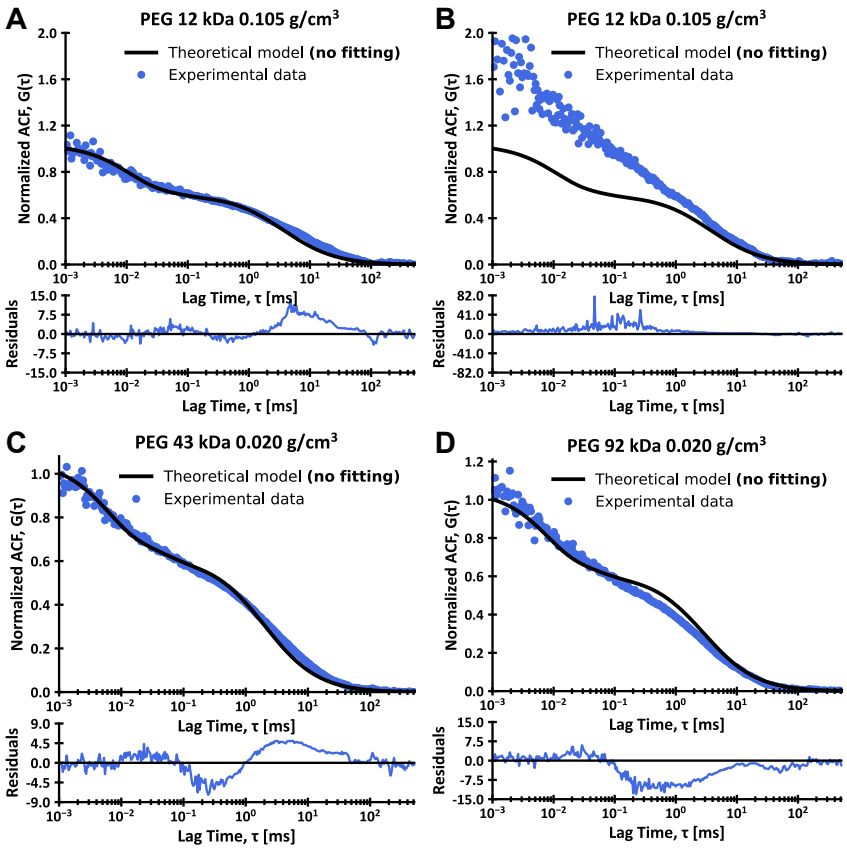

Figure S6. *FCS data for single Alexa 647 stained CCMV particles in solutions of PEG of various molecular weights in virus buffer at 25 °C and calculated theoretical curves, with plots of residues. All presented auto-correlation curves show influence from aggregation of the viruses. (**A**) Data for 0.105 g/cm^3 solution of PEG 12 kDa in virus buffer. The sample measured immediately after preparation. (**B**) Data for the same sample as (**A**) but measured 10 min later. The experimental data from (**B**) was normalized using the same normalization constant as data displayed at (**A**), to preserve the relative amplitudes of the auto-correlation curves on subfigures (**A**) and (**B**). (**C**) Data for 0.020 g/cm^3 solution of PEG 43 kDa in virus buffer. (**D**) Data for 0.020 g/cm^3 solution of PEG 92 kDa in virus buffer. Data presented as solid lines are **not fits** and were calculated according to Eq. 2, 7-9, 11, and 15. The residuals were calculated as a difference between experimental and theoretical values divided by errors of experimental values for each datapoint. The above-given values of polymer molecular weights are the number average molecular weights.*

2.6 Raw signal for experimental data of CCMV diffusion in polymer solutions

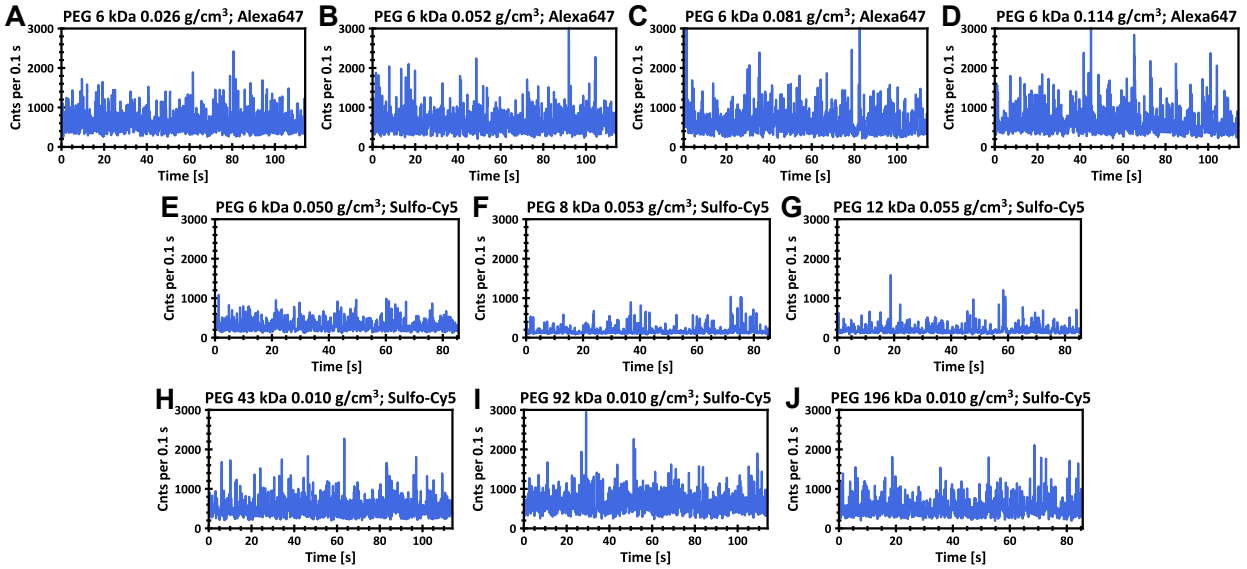

Figure S7. *Fluorescence intensity data for experimental results from Figure 4 and Figure 5. The raw signal was binned to 0.1 s chunks for presentability of the data – the units are photon counts per 0.1 s.*

Figure S7 shows fluorescence intensity (photon count) signal used to calculate the auto-correlation curves on Figures 4 and 5. On all subplots we can observe random fluctuations over average value which means that there is no significant photobleaching of measured samples. In case of photobleaching the signal would decrease in time.

2.7 Staining of ribosomes with Yo-Pro-1

In Yo-Pro-1 stained HeLa cells, the detected average of freely moving molecules is approximately 15 per focal volume, equating to a concentration of about 40 nM. HeLa cells contain roughly 3 million ribosomes per cell,[2] with around 15% represented by free subunits in rapidly dividing cells.[3] This results in a concentration of around 400 nM for each type of free subunit. Free subunits are the only ones detectable by FCS since translation complexes are too large to move freely[4]. Furthermore, with an estimated 10 tRNA molecules for every ribosome in a eukaryotic cell,[5] the concentration of tRNA reaches approximately 27 µM. Consequently, there is almost 1000-fold excess of RNA molecules over Yo-Pro-1 stained molecules. In the given experimental conditions, it is expected that on average each visible RNA molecule is attached to one YO-PRO-1 molecule, with each contributing molecule displaying similar brightness in the FCS signal.

Moreover, the number of available binding sites for free subunits (large ribosomal subunit -LSU, small ribosomal subunit – SSU) and tRNAs also affect the probability of staining these molecules by Yo-Pro-1. As the LSU have much higher number of binding sites than SSU it is expected that there will be a significant excess of Yo-Pro-1 stained LSU as compared to Yo-Pro-1 stained SSU. That is why, the contribution of SSU to the measured FCS auto-correlation curves can be neglected.

On the other hand, while the number of binding sites of tRNA is orders of magnitude lower than for LSU, their concentration is much higher, and their apparent brightness is also higher than for LSU. This results from the rotation time of a molecule affecting its perceived brightness. According to Aragón & Pecora

(1975),[6] a fluorophore can only absorb a photon when its spatial orientation aligns with the polarized laser beam at a certain angle. Therefore, the likelihood of detecting fluorescence from a single fluorophore-labelled molecule is inversely related to its rotation time – faster rotating molecules appear brighter. tRNA molecules rotate three orders of magnitude faster than ribosomal subunits, significantly increasing the chance of detecting photons from a single-stained tRNA molecule over an rRNA molecule. As such we expect the tRNAs to visibly contribute to FCS data.

2.8 Characterisation of tRNAs

We measured the tRNA size by performing FCS in buffer (PBS) at 36 °C. We used commercially available mixture of tRNAs (Transfer Ribonucleic Acid, MP Biomedicals™; Thermo Fisher Scientific) and stained them with 40 nM Yo-Pro-1. The resulted hydrodynamic radius was **2.0 ± 0.1** nm, which was an average of all types of tRNAs in the sample. The FCS curves were fitted with one-component free diffusion model (only translational diffusion, no triplet state dynamics, or other processes), which suggest monodispersity of the sample. tRNA consists of a conserved number of nucleotides and molecular mass of 26 kDa. The variability can result from single amino acids transported by given tRNA, which have masses in the range of 57 Da (Glycine) to 186 Da (Tryptophan). Therefore, the highest possible difference in mass between tRNAs is 0.5 %, thus in terms of applied techniques we consider population of tRNAs as monodisperse.

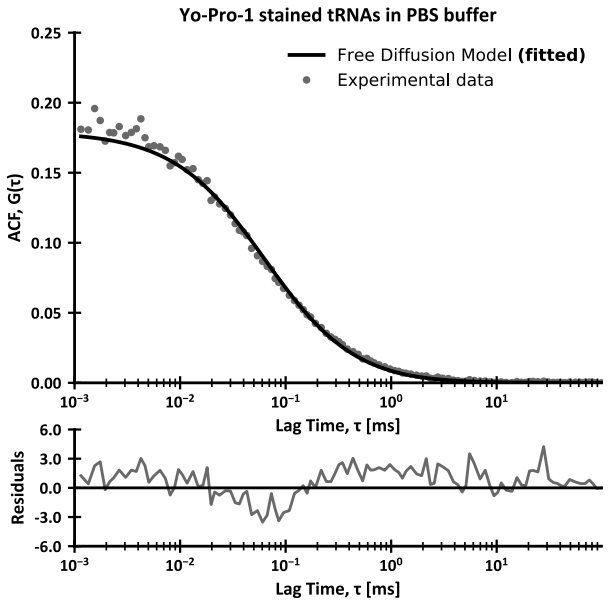

Figure S8. *Example of FCS data for Yo-Pro-1 stained tRNAs in PBS buffer (water viscosity) at 36 °C. The experimental results we fitted with one-component free diffusion model.*

2.9 Calculation of length-scale viscosity for HeLa cytoplasm and nucleus

Eq. S6[7] gives the LSVM for living HeLa cells cytoplasm:

$$\eta_{eff}^{T}(r) = \eta_0 A \exp\left[\left(\frac{\xi^2}{{R_h}^2} + \frac{\xi^2}{r^2}\right)^{-\frac{a}{2}}\right] \quad \text{(S6)}$$

Where A is a preexponential factor on the order of 1, a is a constant in the order of unity, η_0 is the viscosity of the water. $R_h$and ξ are system-characteristic length scales. R_h can be interpreted as a hydrodynamic

radius of the main crowder, while ξ can be interpreted as an effective intercrowder gap. Applying Eq. S6 to Eq. 6 gives us effective viscosity for rotational motion in living HeLa cytoplasm:

$$\eta_{eff}^{R}(r) = \eta_0 A \exp\left[\left(\frac{\xi^2}{{R_h}^2} + \frac{\xi^2}{r^2}\right)^{-\frac{a}{2}}\right]\left[1 + a\left(\frac{\xi}{r}\right)^2\left(\frac{\xi^2}{{R_h}^2} + \frac{\xi^2}{r^2}\right)^{-\left(\frac{a}{2}+1\right)}\right]^{-1} \quad \text{(S7)}$$

The LSVM for living HeLa cells nucleus is given by Eq. S8:[8]

$$\eta_{eff}^{T}(r) = \eta_0 A \exp\left[b\left(\frac{\xi^2}{{R_h}^2} + \frac{\xi^2}{d^2 r^2}\right)^{-\frac{a}{2}}\right] \quad \text{(S8)}$$

Where A is a preexponential factor on the order of 1, a is a constant larger than 1, η_0 is the viscosity of the water, and b is a constant related to the electrostatic interaction between proteins. $R_h$and ξ are system-characteristic length scales. R_h can be interpreted as a hydrodynamic radius of the main crowder, while ξ can be interpreted as an effective intercrowder gap. d is a correction for the caging effect occurring in the systems consisting of hard, non-entangled spheres. Applying Eq. S8 to Eq. 6 gives us effective viscosity for rotational motion in living HeLa nucleus:

$$\eta_{eff}^{R}(r) = \eta_0 A \exp\left[b\left(\frac{\xi^2}{{R_h}^2} + \frac{\xi^2}{d^2 r^2}\right)^{-\frac{a}{2}}\right]\left[1 + ab\left(\frac{\xi}{dr}\right)^2\left(\frac{\xi^2}{{R_h}^2} + \frac{\xi^2}{d^2 r^2}\right)^{-\left(\frac{a}{2}+1\right)}\right]^{-1} \quad \text{(S9)}$$

Table S3. *Values of constants used for calculations of LSVMs for living HeLa cytoplasm and nucleus.*[7,8]

LSMV	A	a	R_h [nm]	ξ [nm]	b	d
HeLa cytoplasm	1.3	0.62	12.9	3.16	-------	-------
HeLa nucleus	1.4	1.29	3.2	24	18.8	1.2066

References

1. Wisniewska, A., Sozanski, K., Kalwarczyk, T., Kedra-Krolik, K. & Holyst, R. Scaling Equation for Viscosity of Polymer Mixtures in Solutions with Application to Diffusion of Molecular Probes. *Macromolecules* **50**, 4555–4561 (2017).
2. Duncan, R. & Hershey, J. W. Identification and quantitation of levels of protein synthesis initiation factors in crude HeLa cell lysates by two-dimensional polyacrylamide gel electrophoresis. *J Biol Chem* **258**, 7228–7235 (1983).
3. Zenklusen, D., Larson, D. R. & Singer, R. H. Single-RNA counting reveals alternative modes of gene expression in yeast. *Nat Struct Mol Biol* **15**, 1263–1271 (2008).
4. Kwapiszewska, K. *et al.* Nanoscale Viscosity of Cytoplasm Is Conserved in Human Cell Lines. *J Phys Chem Lett* **11**, 6914–6920 (2020).
5. Waldron, C. & Lacroute, F. Effect of growth rate on the amounts of ribosomal and transfer ribonucleic acids in yeast. *J Bacteriol* **122**, 855–865 (1975).
6. Aragón, S. R. & Pecora, R. Fluorescence correlation spectroscopy and Brownian rotational diffusion. *Biopolymers* **14**, 119–137 (1975).

7. Kwapiszewska, K. *et al.* Determination of oligomerization state of Drp1 protein in living cells at nanomolar concentrations. *Sci Rep* **9**, 5906 (2019).

8. Bubak, G. *et al.* Quantifying Nanoscale Viscosity and Structures of Living Cells Nucleus from Mobility Measurements. *J Phys Chem Lett* **12**, 294–301 (2021).